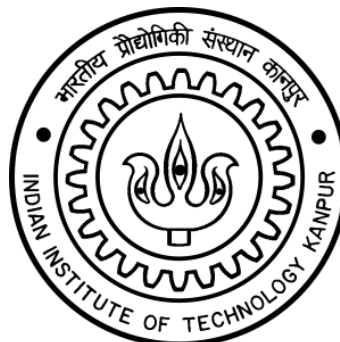

Molecular Dynamics Study on the Welding of Thermoplastics

*A thesis submitted in partial fulfilment of the requirements
for the degree of Master of Technology*

by

Ishu Aggarwal



DEPARTMENT OF MECHANICAL ENGINEERING
INDIAN INSTITUTE OF TECHNOLOGY, KANPUR

June 2019

Certificate

It is certified that the work contained in this thesis entitled “Molecular Dynamics Study on the Welding of Thermoplastics” by “Ishu Aggarwal” has been carried out under my supervision and that it has not been submitted elsewhere for a degree.

Dr. Sumit Basu

June 2019

Professor

Department of Mechanical Engineering
Indian Institute of Technology, Kanpur

Abstract

Name of the student: **Ishu Aggarwal**

Roll No: **17105070**

Degree for which submitted: **M.Tech.**

Department: **Mechanical Engineering**

Thesis title: **Molecular Dynamics Study on the Welding of Thermoplastics**

Thesis supervisor: **Dr. Sumit Basu**

Month and year of thesis submission: **June 2019**

In this work, firstly, simulation procedures are developed to prepare a welded interface of two amorphous homopolymer blocks (glassy amorphous polyethylene) and to compute the interface strength of the welded joint using molecular dynamics. Next, the effect of a set of parameters on the stress-strain response of a weld interface, is investigated. The parameters under study are welding time, welding temperature, welding pressure, quench rate, and applied strain rate. Furthermore, a realistic amorphous polymer sample containing impurities of repulsive nature (resembling to silicon) and voids on the weld interface, is modeled in LAMMPS molecular dynamics simulator. Finally, the interface strength of the contaminated sample is analyzed for the effects of amount of impurity and its distribution pattern on the interface, and of the variation of welding pressure.

Acknowledgements

I am grateful to my supervisor Dr. Sumit Basu for his continuous support, belief and encouragement that helped me during the crucial moments of my thesis work. The freedom bestowed upon me, allowed me to work at my own pace and maintain the balance between work and life.

Contents

Certificate	i
Abstract	ii
Acknowledgements	iii
Contents	iv
List of Figures	vi
List of Tables	vii
Abbreviations	viii
Symbols	ix
1 Introduction	1
1.1 Literature Survey	2
1.2 Overview of the Thesis	3
2 Methodology	5
2.1 Computational details	5
2.2 Sample Preparation	8
2.3 Welding Simulation Technique	10
2.4 Weld interface strength	11
2.5 Contaminated Sample	12
2.5.1 Contaminants	13
2.5.2 Contaminant modeling	13
2.5.3 Sample Preparation	14
3 Results	17
3.1 Pure welded sample	18
3.1.1 Effect of Welding time	18

3.2	Effect of Welding Temperature	19
3.3	Effect of Welding Pressure	19
3.3.1	$\tau_w = 500$ K	20
3.3.2	$\tau_w = 800$ K	20
3.4	Effect of Quenching Rate	20
3.5	Effect of Strain Rate	20
3.6	Effects of Contaminants	21
3.6.1	Effect of amount and distribution of contaminant atoms	21
3.6.2	Effect of pressure	22
3.7	Configurational Analysis	23
3.8	Fracture Toughness (G_c) Analysis	23
3.9	Mean Square Displacement in centre of gravity, $g_2(t)$ Analysis	24
4	Discussion	27
5	Conclusion and Future Scope	29

List of Figures

2.1	Glass transition temperature, T_g of the sample.	6
2.2	Molecular View	6
2.3	Snapshots of the polymeric system showing (a) a single chain and (b) system containing 160 entangled chains.	9
2.4	Snapshots showing (a) compressed block (b) equilibrated compressed block.	9
2.5	Snapshot of welding sample	10
2.6	Snapshot of welding sample during (a) Equilibration within regions (b) Quenching and (c) stretching.	11
2.7	Schematic explaining the calculation of strain rate.	12
2.8	WCA Potential	14
2.9	Snapshots of contaminated sample.	15
2.10	Contaminated sample during equilibration.	15
2.11	Snapshots of contaminated sample containing 11% impurity atoms in closely packed distribution after quenching.	15
2.12	Snapshots of contaminated sample containing 11% impurity atoms in uniform distribution after quenching.	16
3.1	Effect of welding time variation on the stress-strain response for the weld obtained at 500 K, 1 bar.	18
3.2	Effect of welding temperature variation on the stress-strain response for the weld obtained at 1 bar, 10 ns.	18
3.3	Effect of welding pressure variation on the stress-strain response	19
3.4	Effect of quenching rate variation on stress-strain response for the polymer sample welded at 500 K, 10 ns.	21
3.5	Effect of strain rate variation on stress-strain response for the polymer sample welded at 500 K, 60 ns.	21
3.6	Effect of amount and distribution of contaminant atoms on the stress-strain response of the contaminated sample	22
3.7	Effect of pressure on the stress-strain response of the closely pack contaminated sample with 11% impurity	23
3.8	Uniaxial stretching of pure samples welded under different conditions: initial stage on the left, and final one on the right.	24
3.9	Fracture toughness variation of pure welded sample	25
3.10	$g(2)$ vs time response for 500K, 1 bar sample	26

List of Tables

2.1 Force-Field Parameters	7
--------------------------------------	---

Abbreviations

MD Molecular Dynamics

PE Polyethylene

LAMMPS Large-scale Atomic/Molecular Massively Parallel Simulator

Symbols

T_g Glass Transition Temperature

σ stress tensor

ϵ strain tensor

P Pressure Tensor

T_h Higher Temperature

T_l Lower Temperature

τ_w Welding time

\dot{T} Quench Rate (K/ps)

$\dot{\epsilon}$ Strain Rate (s^{-1})

Dedicated to my lovely family

Chapter 1

Introduction

Thermoplastics and its composite have a wide range of applications in land transportation, aerospace and marine structures, and they are replacing their conventional metallic counterparts. It is primarily due to their superior strength-to-weight and stiffness-to-weight ratios as compared to metals. These specific properties result in reduced weight, increased payload capacity, increased operational range and enhanced mechanical performance of structures. They have high static and fatigue load carrying capacity too as compared to metals. These desirable properties of thermoplastics and its composites make them the most potential candidate for various structural applications in different industries. Therefore, joining of thermoplastic and their composite structures is becoming more crucial.

Most manufacturing industries spend a substantial amount of capital in performing the joining operation on materials. Hence, joining processes need to be well understood and optimized, to achieve better joint properties, that too in minimum time and at minimum cost. Experimental works to optimize the process and its parameters also require huge resources like money, time, rigorous equipments and expertise to get the desired outcomes that could be applied in industry. Therefore, performing simulations which mimic the physical system of joining the materials, as closely as possible, in the virtual environment of simulation software, is better alternative to the experimental studies.

MD simulations have the capability to interpret macroscopic mechanical properties at the atomic-scale. They also offer extensive parametric studies and have the potential to avoid the need for long experiments and expenses which may incur in an experimental study. Experimental study of joining process is expensive and can be hardly achieved due to the high sensitivity of the material at some conditions, such as high temperature, high pressure, and rapid growth of melting and crystallization process.

1.1 Literature Survey

MD simulations were used decades back by Wool et al. (1987), to explain the mechanical characteristics of polymer welding. They conducted studies on the strength of polymer interfaces and found out the relationship between the interface strength and the structure of interface by using the concept of entanglement, especially in microscopic deformation models.

Brown and Russell (1996) investigated that the strength of the interface between two immiscible polymers is controlled by the extent to which chains can couple across an interface. While, for the glassy polymer, if the interface is not very weak, the strength is controlled by the number of chains that crosses the interface and entangles with chains on the opposite side of the interface.

Brown (2001) also studied the effect of interface width on interface toughness. This study shows that the interface toughness remains low for narrow interfaces until the interface width becomes larger than the mean entanglement spacing in the bulk and then climbs rapidly to saturation at an interface width of perhaps three times the entanglement spacing.

Mahajan and Basu (2010)

Pierce et al. (2011) investigated the dynamics of polymers across an interface. In this work, they found that the inter-diffusion of polymers across an interface is dominated by the motion of the chain ends. On the contrary, self-diffusion of polymers in melts during the early stages of diffusion is characterized by the reptation-like motion of chains

in constraining tubes formed by the neighboring molecules.

Ge et al. (2013) studied about the interfacial strength of polymers during thermal welding. Their work explains the dependence of interfacial strength on welding time and reveals that interfacial strength gets saturated to bulk shear strength long before polymers diffuse by their radius of gyration. Further, with the increase in strength, the main failure model changes from the chain pullout at the interface to chain scission, as in the bulk. It was also found that the increase of the interfacial strength before the saturation is found to be proportional to the number of the entanglements between chains from opposite sides.

Another remarkable study by Ge et al. (2014) which shows the dependence of tensile fracture of welded polymer interfaces on miscibility, entanglements, and crazing. They found out that the failure of the bulk polymers starts as craze formation, and then followed by the craze breakdown through the chain scission.

Previous work [*ref] is focused mostly on the effect of density of entanglement of the polymer chains across the interface on the weld-interface strength. In this work, we are interested in studying the effects of welding time, welding temperature, welding pressure, quenching rate and strain rate on the interface strength of a glassy amorphous polymer weld. Effect of impurities and voids/microscopic cracks on the weld-interface, is also analyzed. To accomplish these tasks, molecular dynamics simulator (LAMMPS) is used.

1.2 Overview of the Thesis

In **chapter 2**, firstly, the computational details, i.e., modeling, force field and its parameters of an amorphous polymer are presented. Next, pure sample preparation methodology is detailed, followed by welding simulation technique and weld-interface strength determination. Thereafter, contamination in the weld-interface is dealt with, by explaining the model used, and the sample preparation technique. This methodology gives the idea about how the various molecular dynamics ensembles can lead the joining process to be accomplished. In **chapter 3**, a detailed investigation of the various factors culpable in

the interface strength of the weld is taken into consideration and the results of the various simulations carried out on the amorphous PE sample, to investigate the interface strength, are presented. In **chapter 4**, the obervations of these results are discussed. Finally, in **chapter 5**, the conclusion of the significant give-aways of the work is reported.

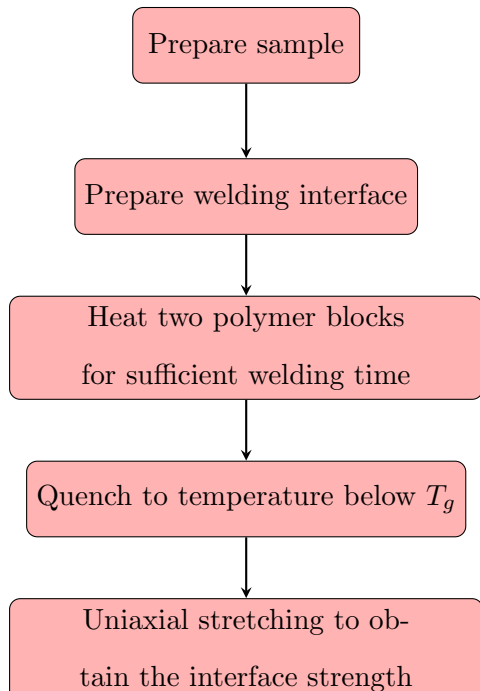
Chapter 2

Methodology

In this chapter, first, the computational details of the modeling and inter-atomic force-field of an amorphous polymer are discussed. Pure sample preparation methodology is detailed next, followed by welding simulation technique and weld-interface strength determination. Thereafter, contamination in the weld-interface is dealt with, by explaining the model used, and the sample preparation technique. The flow-chart here summarizes the methodology involved in this work.

2.1 Computational details

This work uses a dense glass polymer system comprising of 160 entangled macro-molecular chains with 1000 united monomer units per chain, similar to the system used by Mahajan and Basu (2010). Though, the intention here is not to simulate any particular polymer, the inter-atomic force-field for the system is chosen, to resemble that of a coarse-grained



generic amorphous polyethylene (PE) with the monomer unit as CH_2 and end group as CH_3 as outlined by Fukuda and Kuwajima (1997). This atomistic sample is prepared at a temperature below the glass transition temperature T_g , and, then the glassy response is obtained by quenching. Glassy behaviour is confirmed by simulating macromolecular ensemble at 100 K which is well below the T_g (\approx 230K to 250 K), as discussed by Mahajan and Basu (2010). The inter-atomic force field, chosen to model the polymer, is discussed

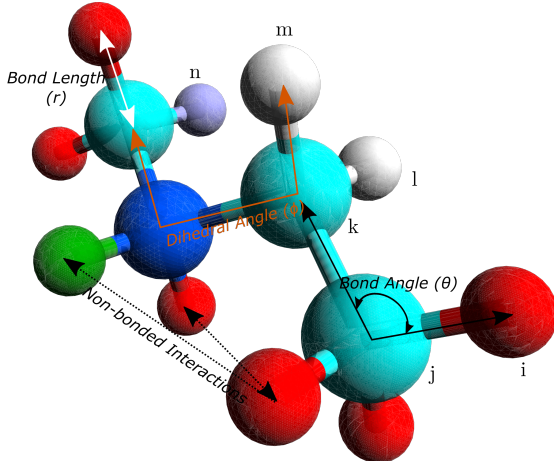


Figure 2.1: Glass transition temperature, T_g of the sample.

Figure 2.2: Molecular View

next.

In this atomistic model of the polymer, the internal energy E comprises of harmonic bond-stretching potential E_b , bond-bending potential E_θ , torsional potential E_ϕ , and, energy E_{nb} due to pairwise non-bonded interactions (Lennard-Jones interactions). Each of these potentials is computed as follows (refer Figure 2.2):

$$\begin{aligned} E_b &= \frac{1}{2} K_b (r - r_0)^2 & E_\phi &= \frac{1}{2} \sum_{n=1}^4 K_n [1 + (-1)^{n-1} \cos n\phi] \\ E_\theta &= \frac{1}{2} K_\theta (\theta - \theta_0)^2 & E_{nb} &= 4\epsilon \left[\left(\frac{\sigma}{r} \right)^{12} - \left(\frac{\sigma}{r} \right)^6 \right] \end{aligned} \quad (2.1)$$

where K_b is bond-stretching stiffness, r_0 is the equilibrium bond length, K_θ is bond-bending stiffness, θ_0 is the equilibrium bond angle. K_1, K_2, K_3 and K_4 are dihedral parameters, ϕ is the dihedral angle. r is the distance between particles. σ is the value of r

upon the number of particles involved. r_i , $i = 1, 2, 3$ are the position coordinates of a particle. v_{ki} , $i = 1, 2, 3$ are the velocity coordinates of the k^{th} particle. Each particle has the same mass m . N_b , and N_{nb} are the number of bonding and non-bonding pairs respectively, in the system. Similarly, N_θ and N_ϕ are the number of triplets and quartets involved in the respective interaction types. V is the system volume.

All simulations are performed in LAMMPS (Plimpton, 1995) which is a parallel molecular dynamics code. Integration of the classical equations of motion uses the velocity verlet algorithm with an integration time step of 1 femtosecond. Nose-Hoover thermostat and Nose-Hoover barostat are used to maintain isothermal and isobaric conditions, respectively. Periodic boundary conditions (PBC) are used in all analyses performed.

In LAMMPS, all computations are performed in real units, which are finally converted to SI units, using an appropriate conversion factor.

2.2 Sample Preparation

A glassy polymeric system of 160 entangled chains with 1000 monomers per chain, is prepared at a temperature below its glass transition temperature T_g (Mahajan and Basu, 2010). For this, firstly, a single chain is prepared (Figure 2.3a), and, then 160 such chains are entangled together to form a polymer block (Figure 2.3b), through a series of steps in between, as discussed by Mahajan and Basu (2010). This preparation is carried out in MATLAB and LAMMPS.

This block is compressed between the two repulsive confining walls moving very slowly towards each other (Figure 2.4a), during canonical (**NVT**) simulation. NVT simulation is performed at a high temperature T_h to attain the homogeneity and eliminate voids. Moreover, proper checks are taken to maintain the theoretical density of the polymer block. Repulsive nature is imparted to the walls by choosing high ϵ and low σ values. These walls are supposed to interact with the atoms present on the surface of polymer blocks by wisely setting the L-J cutoff value r_c , otherwise bulk properties will get affected.

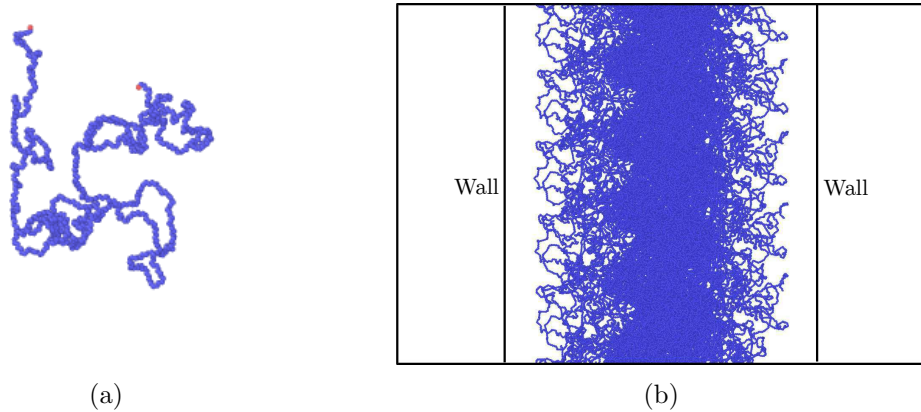


Figure 2.3: Snapshots of the polymeric system showing (a) a single chain and (b) system containing 160 entangled chains.

After the compression, the block is well equilibrated using the isothermal-isobaric (**NPT**) simulation at constant pressure P and at temperature T_h , substantially above T_g . Walls are held in their position, at all times (Figure 2.4b), and only removed once the preparation is complete.

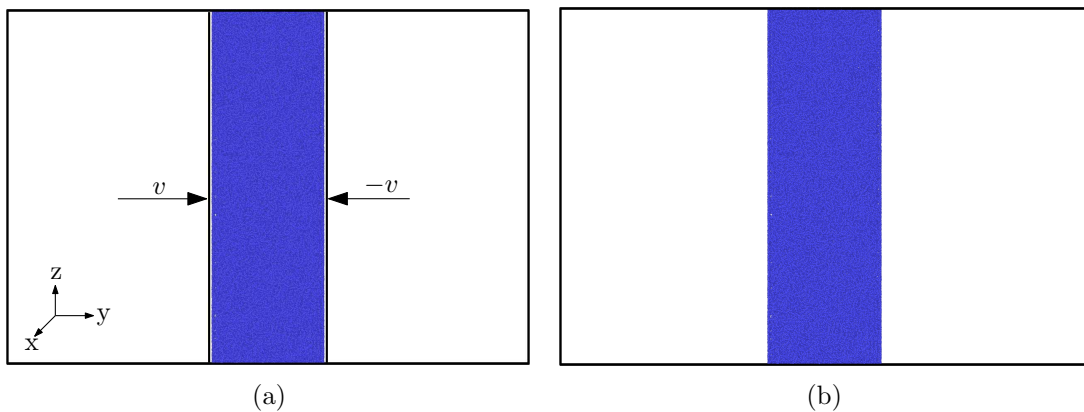


Figure 2.4: Snapshots showing (a) compressed block (b) equilibrated compressed block.

Two polymer blocks are mated against each other with 2 \AA gap, to prepare the welding interface.

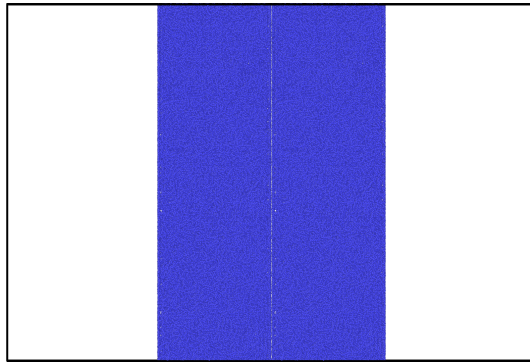


Figure 2.5: Snapshot of welding sample

2.3 Welding Simulation Technique

The welding methodology for thermoplastics is simulated to obtain a welded sample. This is discussed in the following steps. Firstly, welding sample is well equilibrated at constant pressure and constant temperature (higher than T_g) for sufficient welding time. Here NPT ensemble is used to maintain constant temperature T_h and constant pressure P in the system. This equilibration is done in the presence of two fixed block-shaped regions, defined on the left and right sides of the assembly, respectively. These regions are taken from the sample itself (Figure 2.6a). In absence of these regions, the polymer chains would fill the entire box, and consequently, bulk would be simulated instead of separate blocks, because of the periodic boundary conditions applied in all directions.

After equilibration, the regions are removed, and the sample is quenched freely at constant pressure P , at quench rate of \dot{T} , from temperature T_h to T_l which is well below T_g . As both the regions are removed, the sample expands in y-direction. Therefore, the box is expanded to have empty spaces on both the sides of the sample, to avoid bulk simulation. Quenching in this virtual environment is again an NPT simulation. With quenching, the density increases, which is manifested in the shrinkage of the welded sample (Figure 2.6b).

Quench rate is defined as the rate at which the system is cooled rapidly to obtain certain material properties. If the system is cooled from the temperature T_h to T_l in time τ , the quench rate \dot{T} is given by:

$$\dot{T} = \frac{T_h - T_l}{\tau} \quad (2.4)$$

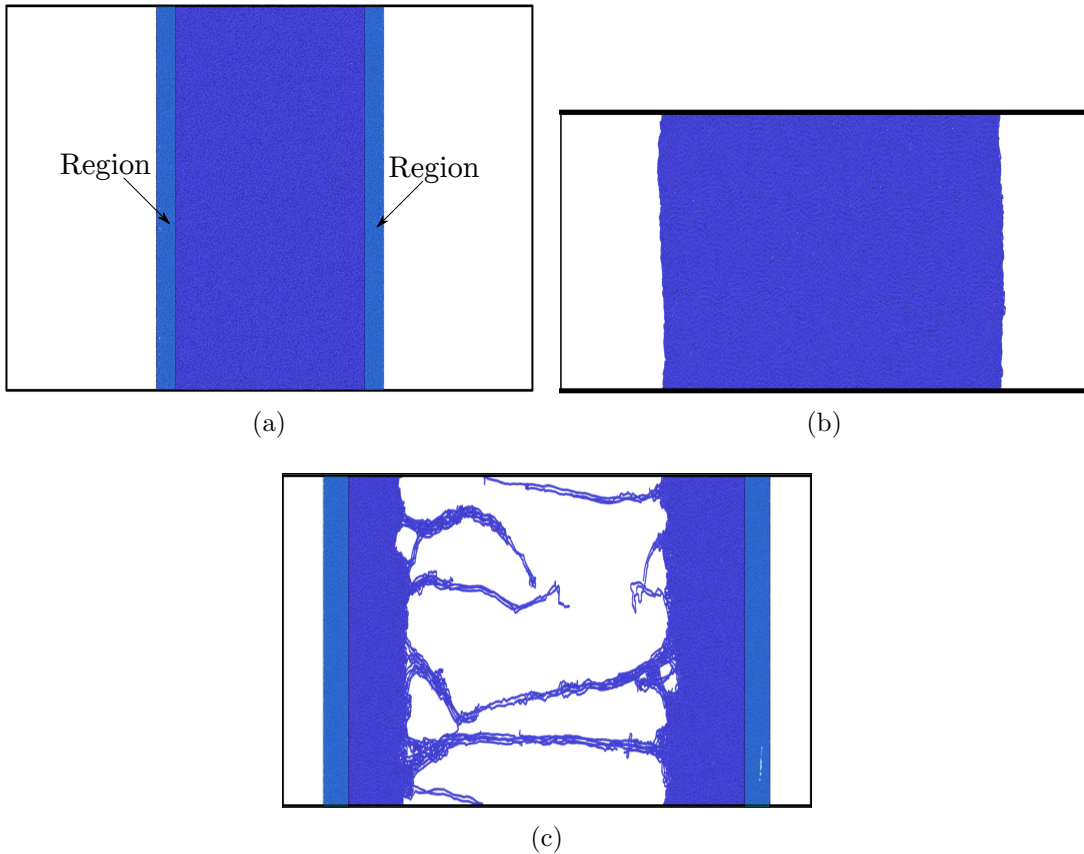


Figure 2.6: Snapshot of welding sample during (a) Equilibration within regions (b) Quenching and (c) stretching.

2.4 Weld interface strength

The weld interface strength is obtained by simulating the uniaxial stretching of the quenched sample. For this, first this quenched sample is provided with movable regions on its both sides. Then, the uniaxial tension is applied in y-direction at the strain rate of $\dot{\epsilon}$ in **NVT** simulation, to obtain the stress strain response and mode of interface failure (Figure 2.6c).

In our simulations, strain rate is provided by imparting equal and opposite velocities v to the two regions using the **velocity** command in LAMMPS.

Let the initial length of the sample be L_i , and the sample be confined between $y = y_i^{(l)}$ to $y = y_i^{(h)}$ (Figure 2.7a). After stretching for time t , the final length of sample becomes L_f , as its ends are now at $y = y_f^{(l)}$ and $y = y_f^{(h)}$. The strain rate $\dot{\epsilon}$ is then, computed as

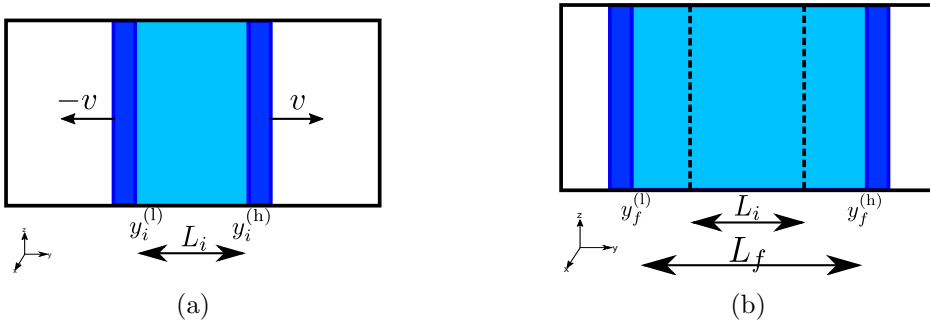


Figure 2.7: Schematic explaining the calculation of strain rate.

follows:

$$\begin{aligned} y_f^{(h)} &= y_i^{(h)} + v * t & L_i &= y_i^{(h)} - y_i^{(l)} & \epsilon &= \frac{L_f - L_i}{L_i} \\ y_f^{(l)} &= y_i^{(l)} + (-v) * t & L_f &= y_f^{(h)} - y_f^{(l)} & \dot{\epsilon} &= \frac{\epsilon}{t} \end{aligned}$$

The dotted lines in Figure 2.7b represent the initial size of the system under consideration.

For computing the stress component σ_{ij} (Eq. 2.2), in LAMMPS, first the stress component per atom is found for each atom, using built-in command **compute stress/atom**. Then, **compute reduce sum** command is used to get the sum over all atoms in the system, which is finally divided by volume V .

All the above shown snapshots are taken using a visualization software, OVITO (Stukowski, 2009).

2.5 Contaminated Sample

In the previous sections, we dealt with ideal amorphous polymers only. But, in reality, no material is ideal. Real polymers contain voids, traces of impurities having either repulsive or attractive nature, and, residuals of other monomer groups. Traces of impurities have low molecular weight such as remnants of solvents, precipitants, catalysts, activators, modifiers, emulsifiers, stabilizers, etc. Residual of monomer groups includes CH_3 , CO , $\text{C}=\text{C}$, $\text{C}-\text{O}-\text{C}$, COOH , etc. These groups are present in the polymer in small quantities,

but, influence its behavior noticeably (Mark, 1948). In polymers, a significant amount of contaminants is introduced as the result of imperfection of their synthesis process.

In spite of these defects, polymers are useful in a wide range of applications due to their low cost, easy availability and low weight. Most of the amorphous polymers have direct and indirect applications. Indirectly, these are used in composites, as a matrix with various types of reinforcements. In composites, contaminants and voids are introduced on their surface, when the release film is peeled off leaving some traces of its release agents on the composite surface (Sacchetti et al., 2017). Direct applications are household and industrial products, manufactured solely from polymers.

2.5.1 Contaminants

In this work, we simulate contaminants of repulsive nature and microscopic cracks/voids in the weld-interface. These defects may appear when polymer blocks to be welded sustain surface asperities while peeling off the release film from their surface, and may also be left with impurity particles on their surfaces as well. Post welding, the impurity particles would be embedded in the interface, and microscopic cracks or void would form therein, due to repulsive nature of the impurity particles. If particles are sparsely distributed, voids would form around the impurity particles. In the case of closely packed particles, microscopic cracks would form around them.

2.5.2 Contaminant modeling

Contaminants are modeled as particles, resembling closely with silicon atoms. Interactions among these particles, as well as, with the surrounding polymer chains, are of non-bonding and repulsive nature. Two arrangement of particles are considered: (i) uniform distribution over the welding interface, and, (ii) closely packed around the center of the interface. First model is used to simulate voids surrounding sparsely distributed impurities in the welded sample. With the second model, microscopic cracks surrounding closely packed impurities in the welded sample are simulated.

The non-bonding interactions are modeled using Lennard-Jones (L-J) potential (Eq. 2.1). Here, a special case of L-J potential is used, namely, the Weeks-Chandler-Anderson (WCA) potential (Heyes and Okumura, 2006). WCA potential is infact, the L-J potential shifted upwards by ϵ and truncated at the minimum point of the L-J potential (which happens at $r = 2^{1/6}\sigma$) (Figure 2.8). This potential E_{WCA} is therefore, given by:

$$E_{\text{WCA}} = \begin{cases} 4\epsilon \left[\left(\frac{\sigma}{r}\right)^{12} - \left(\frac{\sigma}{r}\right)^6 \right] + \epsilon, & r < 2^{1/6}\sigma \\ 0, & r \geq 2^{1/6}\sigma \end{cases}$$

To enforce the repulsive nature of the particles, ϵ is chosen high, σ low, and cutoff radius r_c equal to $2^{1/6}\sigma$ above which there is no interaction between particles. L-J parameters used in this study are as follows: $\sigma = 7.0 \text{ \AA}$, $\epsilon = 0.40 \text{ kcal mol}^{-1}$, mass of atom = $28.0855 \text{ g mol}^{-1}$.

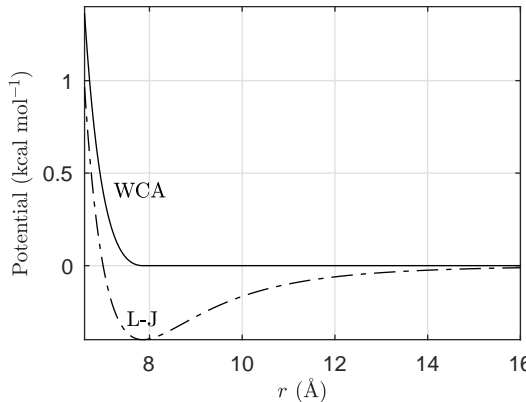


Figure 2.8: WCA Potential

2.5.3 Sample Preparation

The contaminated weld sample is prepared as follows. Firstly, an array of contaminant atoms is prepared in MATLAB. The number of atoms used here is decided by the intended percentage of the welding-interface area covered by them (Figure 2.9a). The array is then, placed in between two polymer blocks shown in Figure 2.4a with a gap of 15 \AA , in LAMMPS (Figure 2.3b). Blocks are next, pushed towards the contaminant atoms, as close

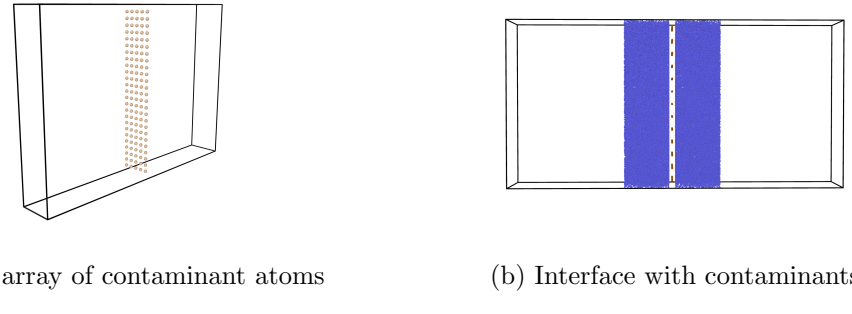


Figure 2.9: Snapshots of contaminated sample.

as possible, at a very low velocity. The contaminant atoms are kept fixed throughout the sample preparation and welding, otherwise, these atoms would diffuse into the polymer bulk, which is not desirable. Now, microcanonical (**NVE**) simulation is run for a short time (0.1 ns) to dampen the velocity present in both blocks, by giving random velocities to the block atoms. The contaminated sample obtained (Figure 2.10) is then, welded as per the procedure given in Section 2.3 and 2.4.

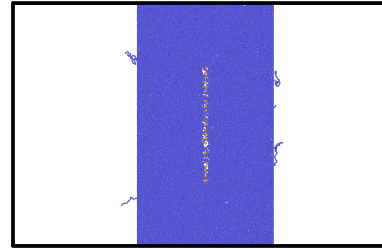


Figure 2.10: Contaminated sample during equilibration.

Figure 2.11 and 2.12 show the opening up of voids and cracks during quenching of contaminated sample, under different pressure values and distributions.

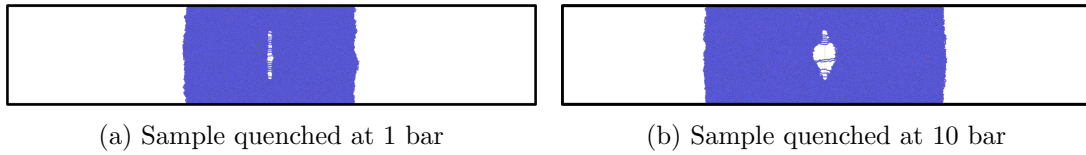


Figure 2.11: Snapshots of contaminated sample containing 11% impurity atoms in closely packed distribution after quenching.

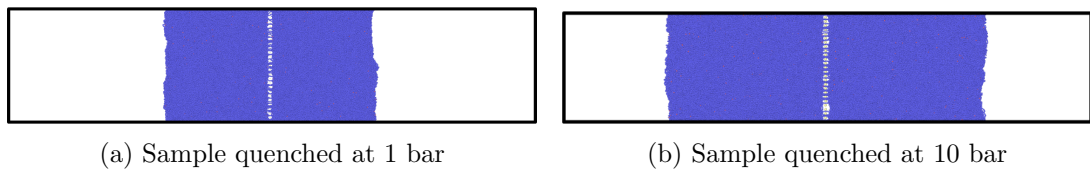


Figure 2.12: Snapshots of contaminanted sample containing 11% impurity atoms in uniform distribution after quenching.

Chapter 3

Results

In this chapter, the stress-strain response for welded pure sample is presented to demonstrate the effect of various parameters viz. welding time, welding temperature, welding pressure, quenching rate and strain rate. Further, the change in the response, due to variation in the welding pressure, is also observed for the contaminated sample, at different impurity levels.

In all simulations, quenching rate and strain rate are set to 1.5 K ps^{-1} and 10^{10} s^{-1} respectively, unless stated otherwise. Uniaxial stress testing is performed at 1 bar pressure and 100 K temperature. Although this strain rate is very high and seems unrealistic, yet it is used, to limit the simulation runtime which would otherwise be of several months on the HPC available at IIT Kanpur.

The simulations in this work are performed on the High Performance Cluster (HPC) at Computer Center, IIT Kanpur and Chicago cluster in Computational Mechanical Lab, IIT Kanpur. The HPC is configured with 1 CPU and 786 GB of RAM, while the Chicago cluster has 192 cores and 128 GB of RAM.

The sections ahead, present the various results obtained.

3.1 Pure welded sample

3.1.1 Effect of Welding time

The interface strength of the pure welded sample, for different welding times, is compared with the bulk response, through the stress-strain curves obtained from uniaxial testing. Here, welding is simulated at 500 K temperature, and 1 bar pressure. The welding time is varied between 0 ns to 60 ns, in steps of 10 ns.

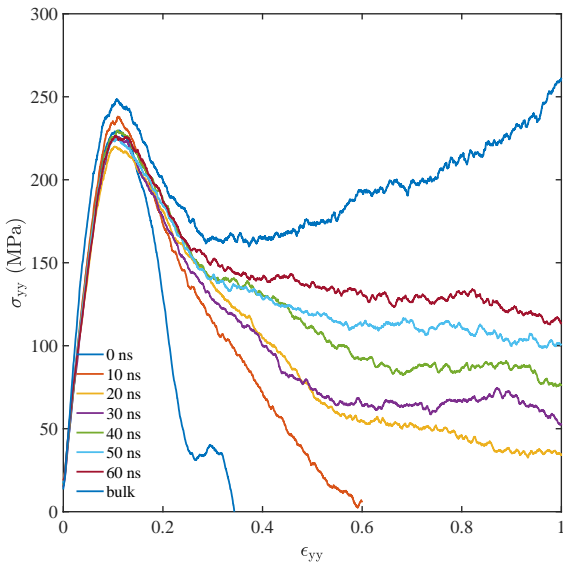


Figure 3.1: Effect of welding time variation on the stress-strain response for the weld obtained at 500 K, 1 bar.

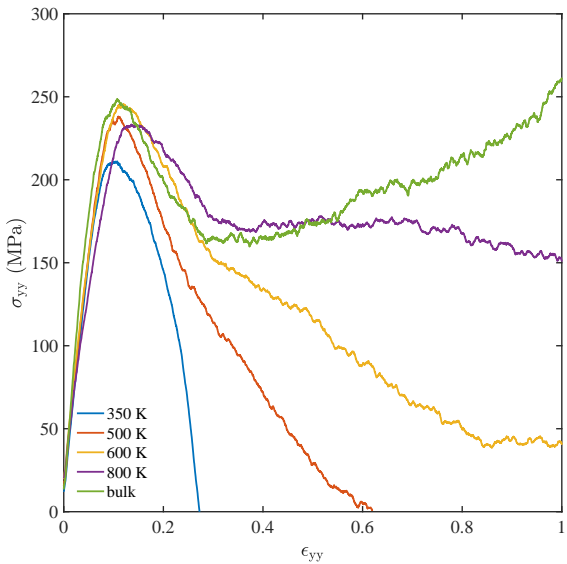


Figure 3.2: Effect of welding temperature variation on the stress-strain response for the weld obtained at 1 bar, 10 ns.

It is observed in Figure 3.1 that the stress-strain curve follows the bulk response upto $\epsilon_{yy} = 0.15$, and, thereafter saturates to different values. The saturation values (strain-hardening response) increase uniformly with the weld time, approaching towards the bulk response. This behavior (strain-hardening) is unlike the gradual increase observed in the bulk response.

The results indicate that, the weld interface strength improves with the increase in the welding time.

3.2 Effect of Welding Temperature

Figure 3.2 compares the stress-strain behavior for different welding temperatures viz. 350 K, 500 K, 600 K and 800 K (all well above the T_g of the polymer). Here, the sample is equilibrated at 1 bar pressure for the welding time of 10 ns. The interface strength is observed to improve with increase in the welding temperature. The yield strength is almost the same for all temperature values, except for 350 K in which, it is slightly lower. Strain hardening and plasticity increase continuously with temperature. With increase in temperature, the stress-strain response is seen to approach the bulk response.

3.3 Effect of Welding Pressure

The interface strength is compared for two different welding pressure values of 1 bar and 10 bar. The sample is equilibrated for 10 ns of welding time, at the welding temperature of 500 K. Another sample is equilibrated at 800 K, to observe whether the response changes at a higher temperature.

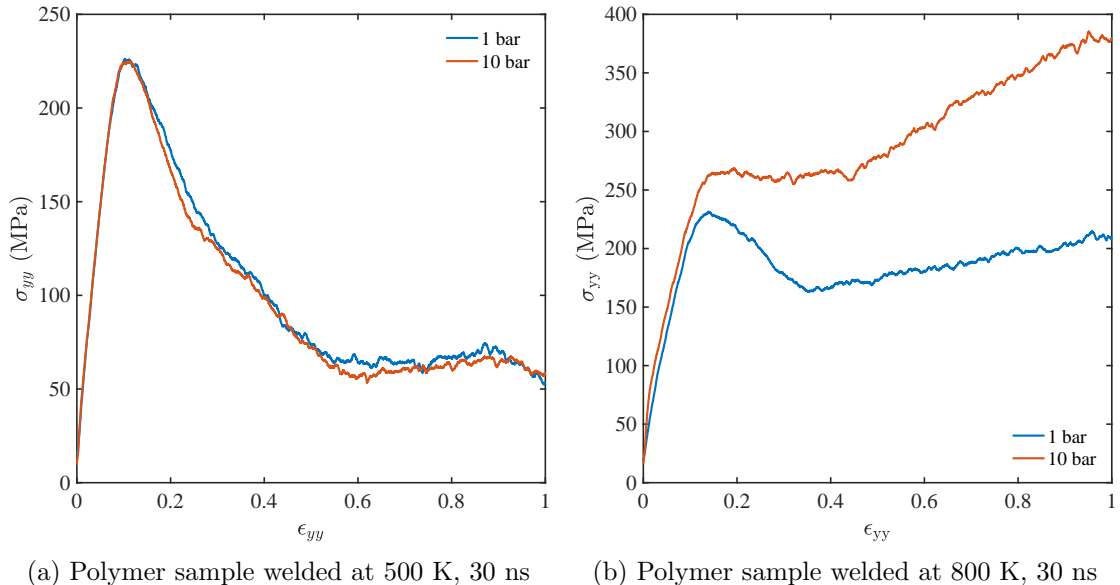


Figure 3.3: Effect of welding pressure variation on the stress-strain response

3.3.1 $\tau_w = 500$ K

As seen in Figure 3.3a, at the lower welding temperature (500 K), stress-strain responses for 1 bar and 10 bar are similar. Thus, at low welding temperature, the interfacial strength of the weld is almost independent of pressure.

3.3.2 $\tau_w = 800$ K

Figure 3.3b shows that, at the higher welding temperature (800 K), the effect of welding pressure is more pronounced. At the higher pressure value, both yield strength and strain hardening are more, in comparison to the lower one. This confirms that, at higher temperature, increasing weld pressure is advantageous in achieving higher interface strength. Further, the stress-strain response is of gradually increasing nature like the bulk response, which was never obtained previously.

3.4 Effect of Quenching Rate

Quenching rates of 1.5 K ps^{-1} and 0.15 K ps^{-1} are used to obtain two weld samples equilibrated at 500 K, 1 bar, and welding time of 10 ns. Stress-strain curve reveals that (Figure 3.4), at higher quenching rate, the interface strength is observed to be much larger. Oscillatory response is observed in the case of the higher quenching rate.

3.5 Effect of Strain Rate

In this study, the strain rate is lowered to 10^9 s^{-1} from the default value of 10^{10} s^{-1} , to observe if the stress-strain response is altered. The equilibration is performed at 500 K, 1 bar, for 60 ns. Figure 3.5 indicates that, a higher strain rate results in better weld interface strength, both in terms of yield strength and strain hardening.

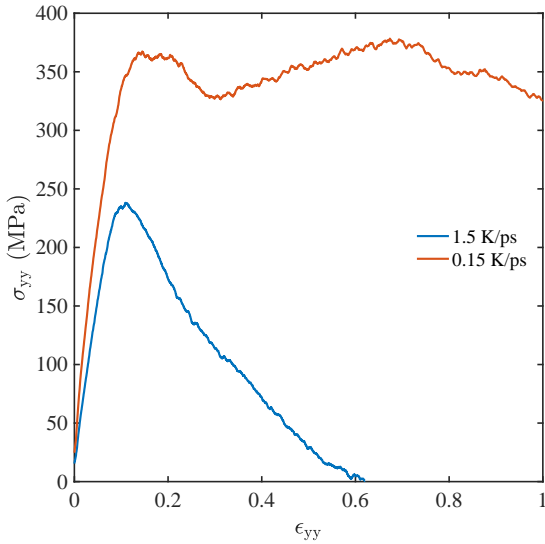


Figure 3.4: Effect of quenching rate variation on stress-strain response for the polymer sample welded at 500 K, 10 ns.

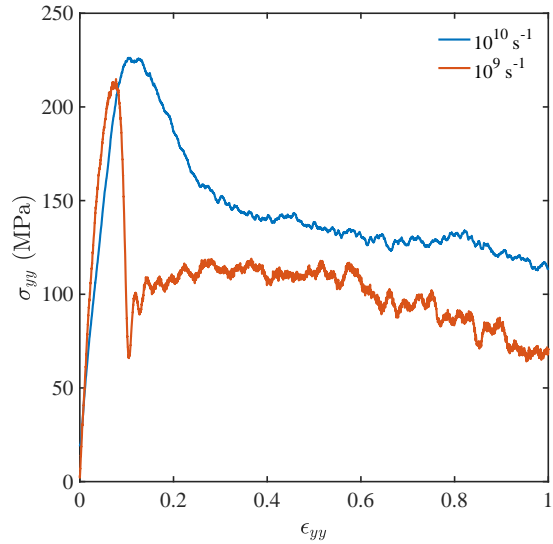


Figure 3.5: Effect of strain rate variation on stress-strain response for the polymer sample welded at 500 K, 60 ns.

3.6 Effects of Contaminants

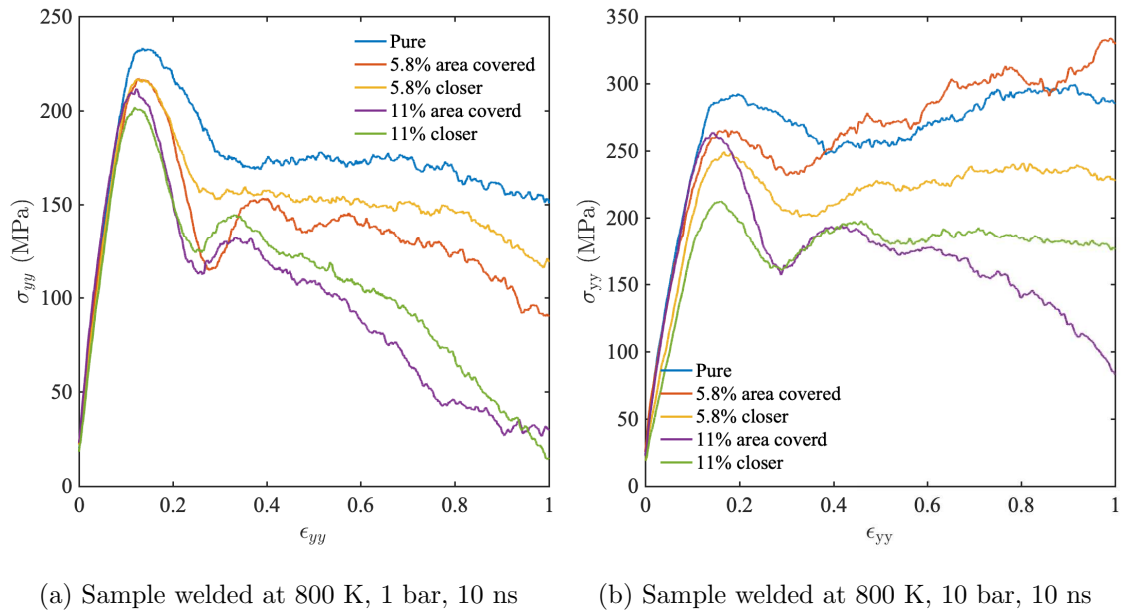
Figure 3.6a and 3.6b show the effect of contaminants on the stress-strain behavior of two different samples equilibrated at 800 K, for welding time of 10 ns, one at the welding pressure of 1 bar, and, the other at 10 bar. The weld interface strength, in general, is observed to decrease with the induction of contaminant atoms on the interface.

3.6.1 Effect of amount and distribution of contaminant atoms

The weld interface strength is investigated for different amount of contaminant atoms. Further, two different distributions of the impurity are considered: (i) uniform distribution, (ii) close packing.

Figure 3.6a shows that, at lower pressure (1 bar), the yield strength and strain hardening both reduce with increase in the amount of contamination. This reduction is observed larger in case of uniform distribution. In case of higher impurity, strain hardening drops significantly.

At higher pressure (10 bar, Figure 3.6b) also, drop in the strength is observed. However, in case of lower impurity (5.8%) with uniform distribution, the strength is observed to be even higher than that of the sample without any impurity. Further, in case of the higher impurity level, the trend gets reversed with respect to the distribution. The yield strength also drops considerably at higher impurity levels.



(a) Sample welded at 800 K, 1 bar, 10 ns (b) Sample welded at 800 K, 10 bar, 10 ns

Figure 3.6: Effect of amount and distribution of contaminant atoms on the stress-strain response of the contaminated sample

3.6.2 Effect of pressure

Figure 3.7 shows the similar trend, as of pure sample. In contaminated sample, at higher temperature (800 K) and pressure (10 bar), yield strength and strain hardening becomes more, compared to the lower one. In this sample, the effect of pressure is more pronounced compared to pure sample.

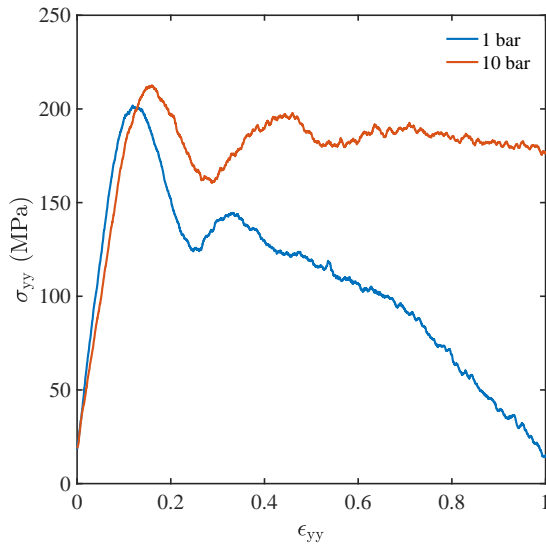


Figure 3.7: Effect of pressure on the stress-strain response of the closely pack contaminated sample with 11% impurity

3.7 Configurational Analysis

Pictorial representation of various configurations at some fixed time-steps shows how the weld interface strengthen with holding time and temperature. Figure 3.8 shows the snapshots of weld samples at different welding times, welding temperature and welding pressure. These snapshots are taken at 3 different stages: (i) initial stage i.e., beginning of stretching (ii) mid-way, i.e., after half of stretching is over and, (iii) final stage.

Figure 3.8a shows that for unwelded sample, interface failure is very neat, as this should be. Figure 3.8b represents that after sufficient welding time (60 ns), interface develops enough strength and mode of interface failure seems to be chain pullout. Figure 3.8c shows that at higher temperature (800 K), interface strength recovers at faster rate compared to lower temperature and interface failure looks like as of bulk.

3.8 Fracture Toughness (G_c) Analysis

Figure 3.9 shows the variation of fracture toughness with welding time and welding temperature. This can be observed from following cases that the fracture toughness of amorphous

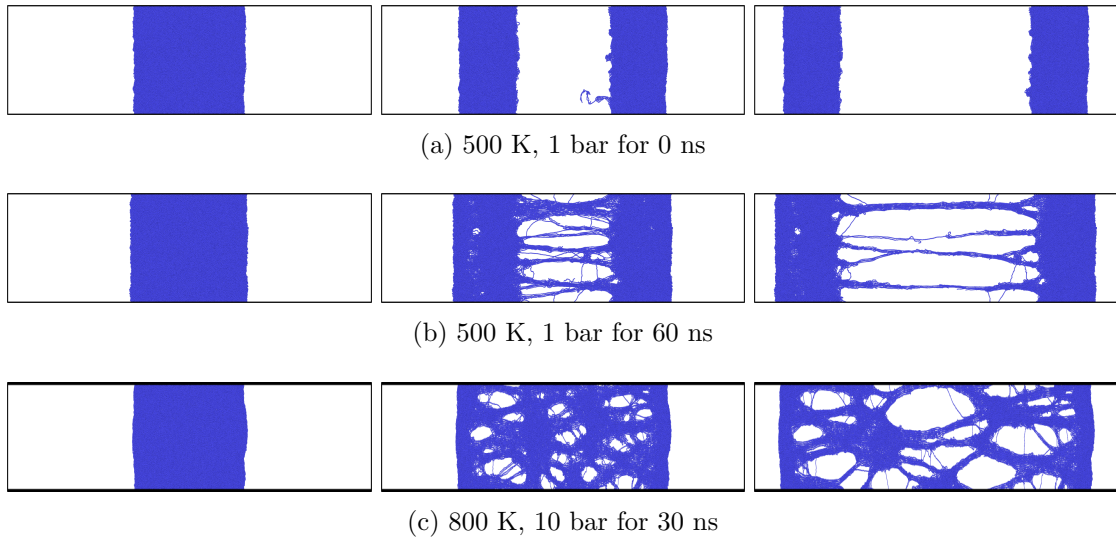


Figure 3.8: Uniaxial stretching of pure samples welded under different conditions: initial stage on the left, and final one on the right.

polymer increase rapidly upto certain temperature and the saturates. Similarly, for time variation at a particular temperature, fracture toughness saturates with increase in time. and time.

3.9 Mean Square Displacement in centre of gravity, $g_2(t)$ Analysis

The mean square displacement of the centre of gravity of polymer chains ($g_2(t)$) with time, at 500 K and 1 bar is computed in this section. Figure 3.10 represents the dynamics of polymer system and investigates the relaxation regime of the polymer system .

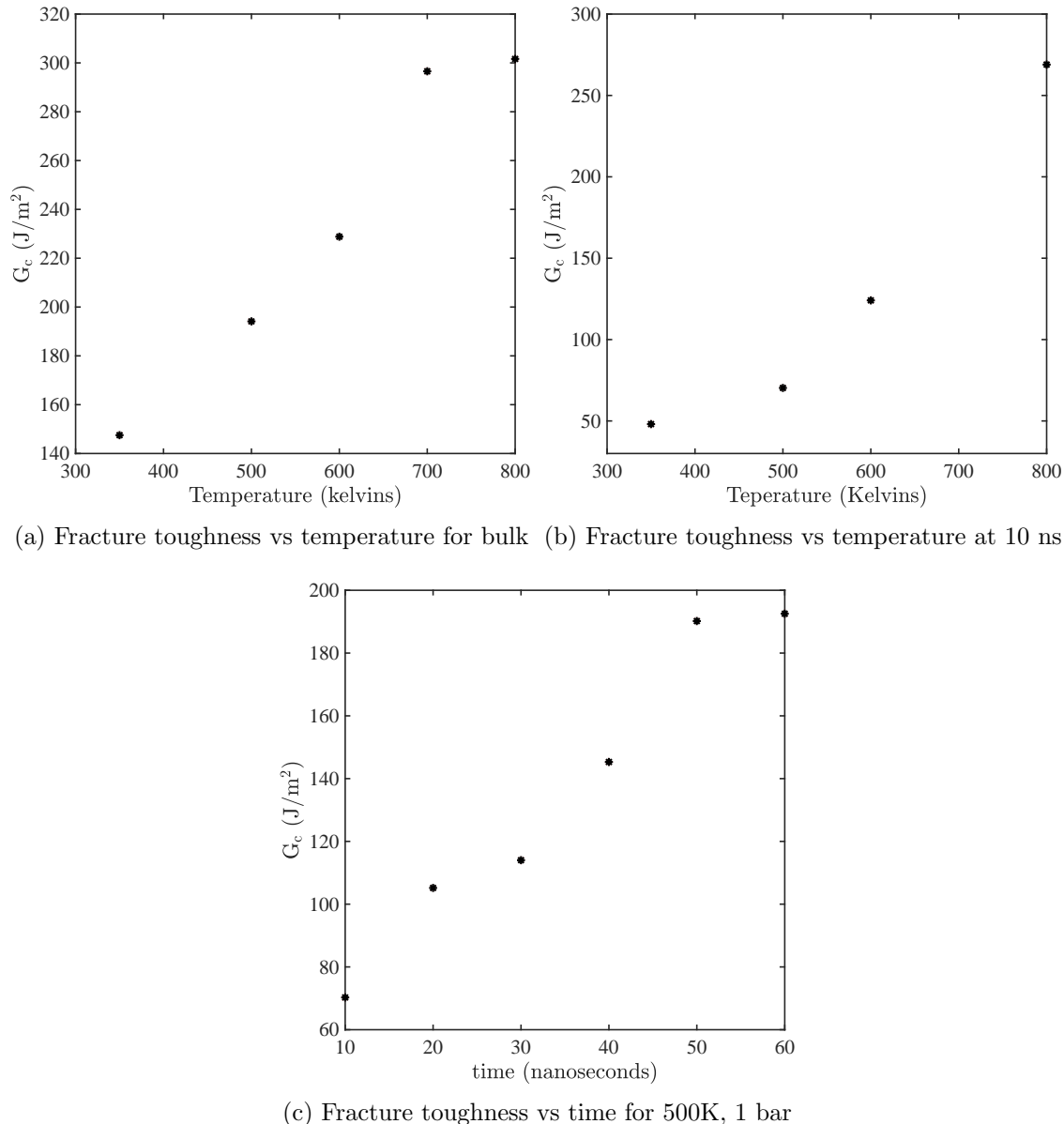


Figure 3.9: Fracture toughness variation of pure welded sample

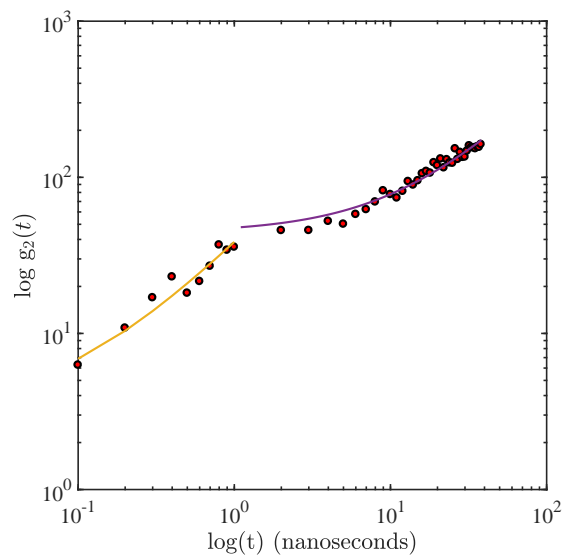


Figure 3.10: $g(2)$ vs time response for 500K, 1 bar sample

Chapter 4

Discussion

Past studies demonstrate that the development of the interface strength during welding is closely related to the formation of entanglement across the interface. Interface becomes mechanically identical to the surrounding portion when bulk entanglement density is recovered at the interface.

To form entanglements, polymer chains inter-diffuse among each other, across the interface. This inter-diffusion of polymer chains is strongly controlled with the welding time. As the welding time increases, polymers chains have inter-penetrated far enough across the interface, and correspondingly the effort required for interface failure is high enough to bond break. Hence, the weld interface strength improves with time and once the bulk entanglement density is recovered, it saturates. And the similar response of stress-strain curve, especially up to ϵ_{yy} , is due to Vander Waal (LJ) interactions (Figure 3.1). Also, at low welding temperature and short welding time, interface failure occurs immediately with the onset of stretching. After failure, only virial stresses remains in the system which results in the wavy nature of stress-strain response.

At high temperature, polymer system have more total energy which is supposed to increase the mobility of the polymer chains, which results in faster inter-diffusion and deeper penetration across the interface. Therefore, the weld interface strength recovers faster with temperature (Figure 3.2).

** Effect of pressure to be discussed.

Quench rate in polymers is very delicate parameter, as it controls the dynamics of polymers chains, especially relaxation mechanism and relaxation mode. Effect of quench rate is a physical effect in the way that a slow quench rate is similar to aging of the polymer. Here, slowly quenched sample has large yield strength and more strain-hardening (Figure 2.6b). This behaviour is quite analogous to the metals, as annealing induces ductility while quenching makes it brittle.

Another reason presented by in (** basu and negi) is that faster quenching locks dihedral conformations into non-equilibrium conformations and does not allow conformational jumps to occur. Vorselaars et al. [2009] have proposed that slower cooled samples produce stronger L-J bonds which can carry a larger load and lead to a sharper yield drop when they break.

Increase in yield strength with strain rate seems to be expected (Figure 3.5). At such a high strain rate value 10^{10} s^{-1} , response of material is not under quasi-static conditions but an impulsive one. So, here interface failure may be thought of as bond stretching instead of chain pullout.

Presence of contaminants, voids and micro-cracks at the interface of the polymer weld, reduces its interface strength is quite intuitive. As the interface contains the impurity of repulsive nature, this will cause hindrance in inter-diffusion of the polymer chains across the interface. So, less entanglement formation will occur. Likewise, increase in the amount of contaminant atoms will adversely affect the interface strength.

Now, comes to the distribution part, with closely packed distribution, the effect obtained is so a big void instead of many small voids distributed over the interface. Presence of contaminants and voids at interface of the polymer weld affect the strength of weld considerably.

Chapter 5

Conclusion and Future Scope

We have performed precisely formulated MD simulations to understand the stress-strain behavior of glassy amorphous polyethylene under uniaxial tension, under different parameters values. In particular, we emphasized that how the mechanical strength of polymer-polymer weld interface is affected with various parameters.

Bibliography

- Berendsen, H. J. C., Postma, J. P. M., van Gunsteren, W. F., DiNola, A., and Haak, J. R. (1984). Molecular dynamics with coupling to an external bath. *The Journal of Chemical Physics*, 81(8):3684–3690.
- Brown, H. R. (2001). Relation between the width of an interface between two polymers and its toughness. *Macromolecules*, 34(11):3720–3724.
- Brown, H. R. and Russell, T. P. (1996). Entanglements at polymer surfaces and interfaces. *Macromolecules*, 29(2):798–800.
- Fukuda and Kuwajima (1997). Molecular-dynamics simulation of moisture diffusion in polyethylene beyond 10 ns duration. *The Journal of Chemical Physics*, 107(6):2149–2159.
- Ge, T., Grest, G. S., and Robbins, M. O. (2014). Tensile fracture of welded polymer interfaces: Miscibility, entanglements, and crazing. *Macromolecules*, 47(19):6982–6989.
- Ge, T., Pierce, F., Perahia, D., Grest, G. S., and Robbins, M. O. (2013). Molecular dynamics simulations of polymer welding: Strength from interfacial entanglements. *Phys. Rev. Lett.*, 110:098301.
- Heyes, D. M. and Okumura, H. (2006). Some physical properties of the weeks-chandler-andersenfluid. *Journal of Experimental Nanoscience*, 32:45–49.
- Kremer, K. and Grest, G. S. (1989). Dynamics of entangled linear polymer melts. *The Journal of Chemical Physics*, 92(8):5057–5086.

- Laboratories, S. N. (2019). *LAMMPS Documentation*. Sandia National Laboratories.
- Mahajan, D. K. and Basu, S. (2010). On the simulation of uniaxial, compressive behavior of amorphous, glassy polymers with molecular dynamics. *International Journal of Applied Mechanics*, 02(03):515–541.
- Mark, H. (1948). Purity and identity of polymers. *Analytical Chemistry*, 2:104–110.
- Pierce, F., Perahia, D., and Grest, G. S. (2011). Dynamics of polymers across an interface. *EPL (Europhysics Letters)*, 95(4):46001.
- Plimpton, S. (1995). Fast parallel algorithms for short-range molecular dynamics. *Journal of Computational Physics*, 117(6):1–19.
- Sacchetti, F., Grouve, W. J., Warnet, L. L., and Villegas, I. F. (2017). Effects of release media on the fusion bonding of carbon/peek laminates. *Composites Part A: Applied Science and Manufacturing*, 94:70 – 76.
- Stukowski, A. (2009). Visualization and analysis of atomistic simulation data with OVITO—the open visualization tool. *Modelling and Simulation in Materials Science and Engineering*, 18(1):015012.
- Thompson, A., Plimpton, S., and Mattson, W. (2009). General formulation of pressure and stress tensor for arbitrary many-body interaction potentials under periodic boundary conditions. *The Journal of chemical physics*, 131:154107.
- Wool, R. P., Willett, J. L., McGarel, O. J., and Yuan, B. L. (1987). Strength of polymer interfaces. *EPL (Europhysics Letters)*, 28(2):38–39.
- Yousefpour, A., Hojjati, M., and Immarigeon, J.-P. (2004). Fusion bonding/welding of thermoplastic composites. *Journal of Thermoplastic Composite Materials*, 17(4):303–341.